Journal of Power Sources 189 (2009) 1100–1105

Contents lists available at ScienceDirect

Journal of Power Sources

journal homepage: www.elsevier.com/locate/jpowsour

Performance of a proton exchange membrane fuel cell stack with thermally conductive pyrolytic graphite sheets for thermal management

Chih-Yung Wen*, Yu-Sheng Lin, Chien-Heng Lu

Department of Aeronautics and Astronautics, National Cheng-Kung University, Tainan 70101, Taiwan

ARTICLE INFO

Article history:
Received 27 November 2008
Received in revised form
22 December 2008
Accepted 22 December 2008
Available online 31 December 2008

Keywords:
Proton exchange membrane fuel cell stack
Pyrolytic graphite sheet
Thermal management

ABSTRACT

This work experimentally investigates the effects of the pyrolytic graphite sheets (PGS) on the performance and thermal management of a proton exchange membrane fuel cell (PEMFC) stack. These PGS with the features of light weight and high thermal conductivity serve as heat spreaders in the fuel cell stack for the first time to reduce the volume and weight of cooling systems, and homogenizes the temperature in the reaction areas. A PEMFC stack with an active area of 100 cm^2 and 10 cells in series is constructed and used in this research. Five PGS of thickness 0.1 mm are cut into the shape of flow channels and bound to the central five cathode gas channel plates. Four thermocouples are embedded on the cathode gas channel plates to estimate the temperature variation in the stack. It is shown that the maximum power of the stack increase more than 15% with PGS attached. PGS improve the stack performance and alleviate the flooding problem at low cathode flow rates significantly. Results of this study demonstrate the feasibility of application of PGS to the thermal management of a small-to-medium-sized fuel cell stack.

1. Introduction

Environmental concerns such as global warming and the limitation of oil sources have renewed the global interests of research and development of fuel cell technology for transportation and stationary or portable power generation [1]. Among many kinds of fuel cells, the proton exchange membrane fuel cell (PEMFC) is one of the most promising candidates for transportation and portable electric power sources because it operates at low temperatures, offers a fast start-up and shut down time, fast response to changing electric loads and can sustain unlimited thermal cycles. Many innovations of modern materials and technologies, in recent years, have increased the efficiency and reliability (life time and degradation) of PEMFC devices dramatically. A typical hydrogen PEMFC can convert the chemical energy of reactants directly to electric energy with a working temperature from 60 to 100 °C and an efficiency of about 50%, leaving the remaining 50% as waste heat.

An understanding of the thermal management within a PEMFC is of critical importance. A single PEMFC or a stack operates more efficiently at higher operating temperatures due to increased kinetic rates at the reaction areas. However, the proton exchange membranes are vulnerable to burning at elevated temperatures. The waste heat must then be discharged efficiently from the fuel cell to prevent the formation of hot spots on the membrane electrode assembly (MEA) and protect the proton exchange membrane. An excessively high or low temperature on a MEA surface may also lead to membrane dehydration and water condensation (even flooding), respectively, due to the complicated coupling of heat, fluid flow and mass transfer processes within the fuel cell. The problem of thermal management associated with that of water management and mass transport limitations within a single fuel cell and a fuel cell stack has been reported by many experimentalists and theoreticians [2–11]. These issues are even more important to the optimization of a PEMFC stack system. The main purpose of thermal management in a PEMFC is to keep the temperature of a single cell or a stack within the specific range and to maintain a uniform temperature distribution over the MEA surface [7,9,11] in order to increase the efficiency and improve the reliability and durability of the MEA.

Cooling methods to discharge the waste heat are determined mainly by the size of the fuel cell. The size of a PEMFC system can vary from less than 100 W for most portable power sources to few KW for stationary-residential or small transport vehicles, 50–75 KW for cars and 200–250 KW for buses [12]. The reported cooling methods [13] include: (1) convective cooling with cathode oxidant flow; (2) convective cooling with separate air flow; (3) convective water cooling and (4) two-phase cooling with heat spreaders. Currently, forced convection air and water flows are generally adopted as the cooling systems of the PEMFC stacks below 2 KW and above 10 KW, respectively. For PEMFC stacks between 2 and 10 kW, a careful choice is needed regarding whether air or water cooling should be used. These cooling systems, in which separate

* Corresponding author. Tel.: +886 6 2757575x63657; fax: +886 6 2349281.
E-mail address: cywen@mail.ncku.edu.tw (C.-Y. Wen).

0378-7753/$ – see front matter © 2008 Elsevier B.V. All rights reserved.
doi:10.1016/j.jpowsour.2008.12.103

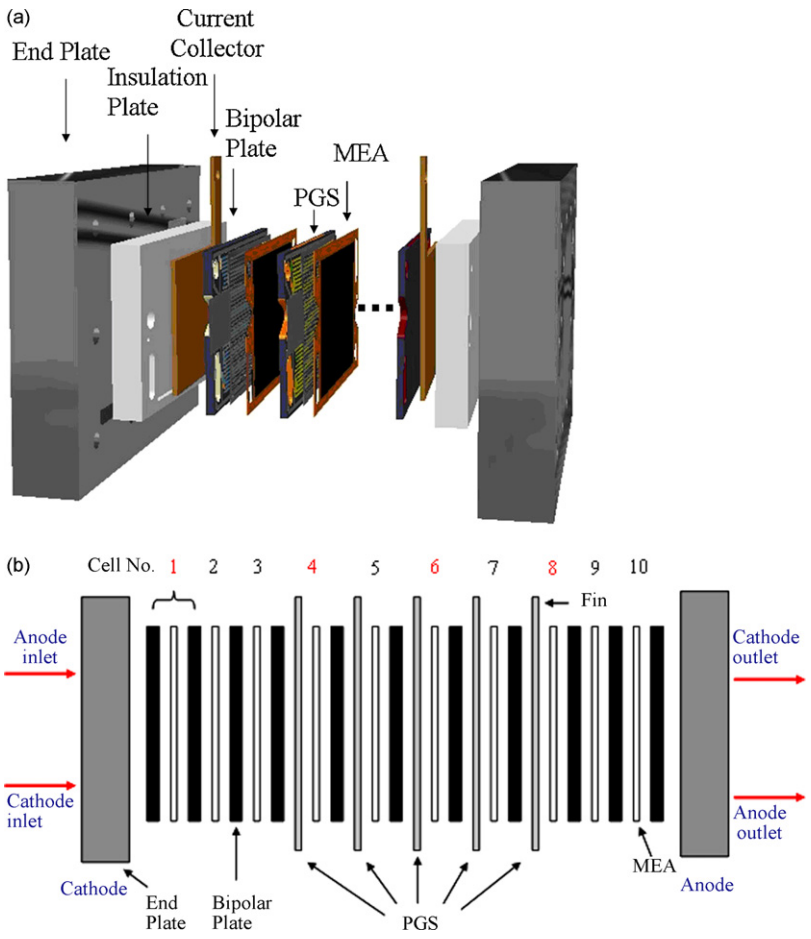

Fig. 1. Schematic of the PEMFC stack: (a) components (b) configuration.

cooling channel plates and a blower or a pump are incorporated, extract around 4–10% of the available electrical power of a PEMFC unit for blowing air or pumping cooling water through the stack to remove the waste heat. For a small fuel cell system, a forced air-cooling system is not preferred because it will extract more (20–25%) of the total power output. The cathode oxidant flow then serves to carry away the heat generated by the reaction as it exits from the PEMFC unit. However, none of the cooling methods with air, water and cathode oxidant flows homogenize the temperature inside a PEMFC unit effectively. The two-phase cooling heat spreaders were suggested to homogenize the temperature inside a PEMFC stack [13,14].

In order to reduce the weight and volume of the thermal management auxiliary system like the two-phase cooling heat spreader and the back work needed to run the system itself, Wen and Huang [15] applied a novel material, pyrolytic graphite sheet (PGS), with high thermal conductivity as a heat spreader to a single PEMFC. PGS was used to transport heat out of the PEMFC through conduction, and then to dissipate this heat to surrounding air through natural convection. The temperature distribution was shown more uniform in the cell with PGS than in the one without PGS. The results demonstrated the promising application of PGS to the optimization of the thermal management of a fuel cell system.

This paper aims to extend our previous work [15] and explore further the feasibility of application of PGS to the fuel cell industry. An experimental investigation of the effects of the PGS on the performance and thermal management of a PEMFC stack is reported for the first time.

PGS is a commercial material synthetically made in a uniform form of highly oriented graphite polymer sheet. PGS is highly thermal conductive, lightweight, flexible and heat-resistant, and has been applied successfully in the thermal management of commercial portable electrical devices like laptop computers, where the spaces are limited [16]. PGS is stable up to about 500 °C and has a thermal conductivity of 600 to 800 $W\,m^{-1}\,K^{-1}$ in the in-plane directions, which is twice that of copper and ten times that of ordinary graphite. Its density is 1.0 $g\,cm^{-3}$, which is 1/9 that of copper and 1/3 that of aluminum. PGS is easy to cut into any shape using simply a pair of hand-held scissors because it is a flexible sheet. All these features of PGS make it a suitable material for providing thermal management and heat-sinking of a PEMFC system and reducing the volume and weight of cooling systems.

2. Experimental

2.1. Design of PEMFC stack with and without PGS

Fig. 1 schematically depicts the fuel cell stack used in our research. The fuel cell stack had 10 single cells assembled in series. Brief details about each component are described in this section. Pelcan® graphite bipolar plates of dimension 155 mm × 85 mm × 2 mm with three-parallel-channel serpentine flow fields for both cathode and anode were used (Fig. 2). Both channel width and height were 1 mm. Both sides of membrane electrode assembly (MEA) were sealed with green silicon rubber sealing-rings placed on the periphery of bipolar plates to ensure gas tight sealing.

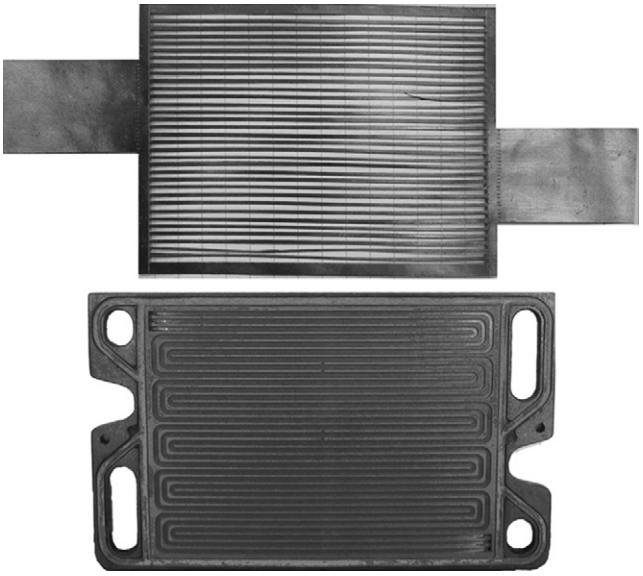

Fig. 2. Picture of the flow channel plate and the shaped PGS.

The MEA (a Nafion® 112 membrane with catalyst loading of anode and cathode: Pt/Ru 0.5 mg cm^{-2} and Pt 0.65 mg cm^{-2}) sandwiched in between two standard TORAY® carbon papers (TGP-H-090) as GDLs were placed in the middle of two flow channel plates. The active area of each MEA was 100 cm^2. End plates were aluminum alloy (6061T651) with dimensions of 250 mm × 180 mm × 20 mm. POM insulation plates and copper current collectors were placed between the end plate and stack. The stack had no external thermal insulation.

During the stack assembly, two positioning rods were used for the alignment. The end plate, insulation plate, current collector, bipolar plate, MEA, etc., were aligned and stacked one by one. Four M10 bolts were used to tighten the stack with a uniform torque of 16 N m. After the assembly, the stack was filled with nitrogen for half an hour to detect any possible leakage.

Five Panasonic®'s PGS (EYGS182310, 0.1 mm in thickness) were cut into the shape of the serpentine flow channels, as shown in Fig. 2, and bound to the five cathode gas channel plates in cells at the center, numbered 4–8 in Fig. 1(b), to evaluate the thermal performance of PGS in the above PEMFC stack. Every trimmed PGS was placed between the cathode channel plate and GDL. The cells at the center are most vulnerable to overheating and sufficient cooling is needed at all times. The two 3.1 cm × 3.1 cm extensions on both sides of PGS to the area of flow channel plate serves as a fin to transfer the heat generated inside the cell by free or forced air convection with the environment (Fig. 1). No fan- and air-cooling channel plates were used in the present study. The simplicity of the hardware makes the PEMFC stack easily fabricated and assembled.

2.2. Experimental set-up

The experimental set-up consists of a gas supply unit, a 10-cell PEMFC stack, a fuel cell test system, 4 thermocouples, a thermocouple data log and a data acquisition system. The computer-controlled Arbin® fuel cell test system (Arbin Instruments, BT2000, 1 kW) composed of an electrical load and a gas handling system was used to control the load and anode and cathode gas parameters. The flow of pure hydrogen from the gas bottle and air from the compressor were regulated by the mass flow controllers inside the gas handling system. The electrodes were purged with nitrogen between two experiments to realize reproducible initial conditions. The fuel cell stack was connected to the electrical load that was operated in constant-voltage discharge mode. The data acquisition system was used to record the current and voltage of the fuel cell stack under operation, gas flow parameters like volume flow rates, relative humidity and temperatures of the air and hydrogen, and thermocouple readings. The experimental set-up supports the simultaneous evaluation of stack performance and temperature distribution in a PEMFC stack under operation. Fig. 3 plots the temperature-measuring point on each one of the cells numbered 1, 4, 6 and 8 in Fig. 1(b) to measure the reference cell temperature (with and without PGS). The temperature distribution of the cell stack is supposed to be approximately symmetric about the center. The temperatures of cell numbered 4, 6 and 8 represent also that of cell numbered 7, 5 and 3, respectively.

2.3. Experimental conditions

The experimental results presented in the next section were gained under the following conditions:

- The MEAs underwent an activation process to ensure that the fuel cell stack has reached a stable status for every test. The process involved running the fuel cell at: (1) 6 V for 60 min; (2) 5 V for 20 min; (3) 7 V for 20 min; (4) open-circuit potential for 30 s.
- The dry hydrogen (<10% RH) gas flow rate was 3 slpm and the temperature was 65 °C.
- The air was humidified to 80% RH at 65 °C.
- The air flow rate was varied from 25 to 35 and 45 slpm, at a temperature of 65 °C and a humidity of 80% RH. The large air flow rates were chosen to assist in carrying away the heat generated by the reaction as it exits from the PEMFC stack and to prevent burning of MEA, especially for the case without PGS. Note that no fan-cooling was used in the present study.
- The atmospheric temperature was 25 °C.

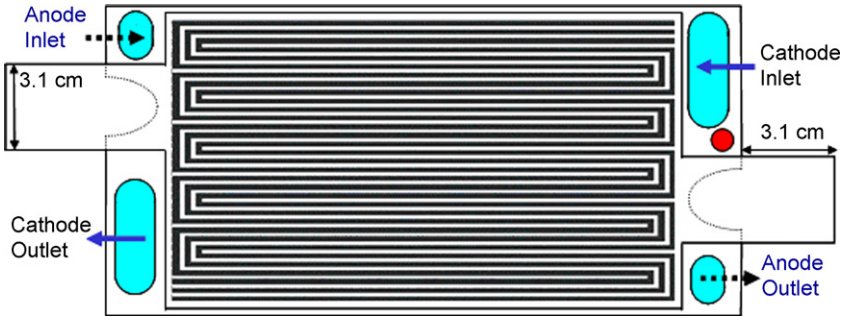

Fig. 3. Schematic of the shaped PGS aligned with the flow channel plate on the cathode and the positions of the temperature measurement points.

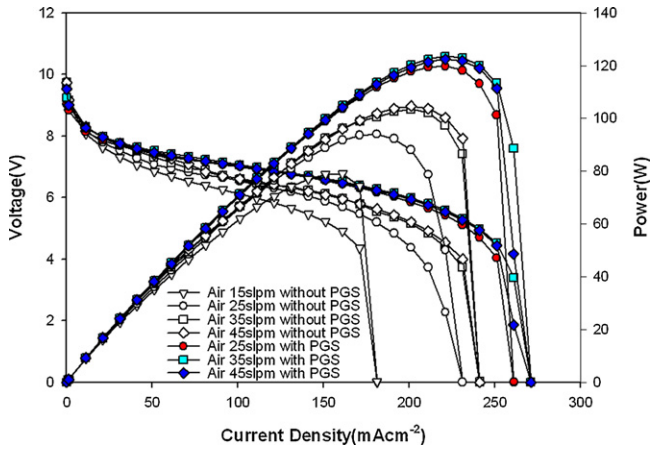

Fig. 4. Polarization curve of the test stack with and without PGS.

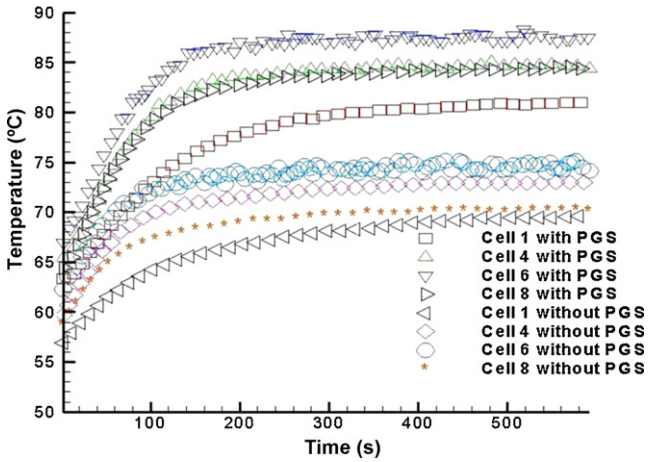

Fig. 5. Typical measured temperatures of the test cells numbered 1, 4, 6 and 8 in Fig. 1 at the air flow rate of 25 slpm. The stack was operated in a constant-voltage discharge mode (5 V).

3. Results and discussion

3.1. Effect of PGS on cell performance

Fig. 4 plots the polarization curve that specifies the performance of the test stack throughout its operating range with and without PGS. The mass transport limitation shifts to higher current densities as the air flow rate becomes larger without PGS. The overall performance of the stack at an air flow rate of 35 slpm is very close to that at 45 slpm. The power density for the air flow rate at 45 slpm is maximal at a current density of about 201.0 mA cm^{-2}, which is higher than the current density reached at an air flow rate of 25 slpm. Increasing the air flow rates removes more water and alleviates the problem of flooding. Also shown in Fig. 4 is the performance of the test stack at an air flow rate of 15 slpm. The mass transport limitation shifts to even lower current density than that at an air flow rate of 25 slpm. Serious flooding was observed when the air flow rate is below 25 slpm in the current experiment setting.

The attachment of PGS to the test stack improves its performance. The mass transport limitation shifts to higher current densities for all the three air flow rates (25, 35 and 45 slpm). The mass transport limitation shifts to higher current densities slightly as the air flow rate becomes larger with PGS. The overall performance of the stack at an air flow rate of 35 slpm is very close to that at 45 slpm. The overall performance of the stack at these three air flow rates is almost the same. The maximum power density is around 120 W at a current density of about 221.0 mA cm^{-2}. The comparison of the maximum power density and the corresponding current density with and without PGS is shown in Table 1. The percentage improvement in the maximum power was calculated by the following equation:

$$(\%)\,\text{improvement} = \frac{\text{maximum power with PGS} - \text{maximum power without PGS}}{\text{maximum power without PGS}} \times 100$$

As seen, that the maximum power of the stack increases 27.4%, 19.3% and 17.6% with PGS attached at air flow rates of 25, 35 and 45 slpm, respectively. PGS improve the stack performance significantly, especially at low cathode flow rates.

3.2. Effect of PGS on cell temperature distribution

The temperature distributions in the stack were estimated by making thermocouple measurements at the specific points on the cells 1, 4, 6 and 8 (Figs. 1(b) and 3). The stack was operated in a constant-voltage discharge mode (5 V) at different air flow rates. This operation voltage is very close to the mass transport limitation. The temperatures were measured after current loading. Fig. 5 plots a typical increase in temperature, with and without PGS (air flow rate of 25 slpm). The activation process described in Section 2.3 yielded the initial temperature distribution (at time zero). The measurements were made for 600 s when all temperatures reached quasi-steady values.

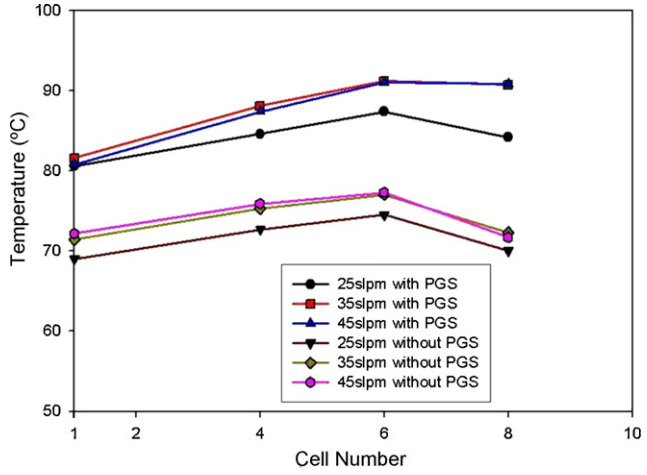

Fig. 6. Quasi-steady temperature distributions in the stack at different air flow rates, with and without PGS.

Fig. 6 presents the quasi-steady temperature distributions in the stack at different air flow rates, with and without PGS. As seen, a variation was found to exist across the stack, with the higher temperatures on the cells at the center. This probably resulted from an insufficient cooling by the small PGS fins (Figs. 2 and 3), even though Wen and Huang [15] has shown that PGS is an effective heat spreader to a single PEMFC and homogenize the temperature inside it. The temperature distribution in the stack with PGS was higher than its counterpart without PGS at every air flow rate. The temperature distributions in the stack at the flow rates of 35 and 45 slpm are nearly the same, with and without PGS. It is well known that the performance of a PEMFC unit is a function of temperature. Increasing of performance with increasing temperature is not only due to increase of the reaction rate of the electrode process but also to an increase of the ionic conductivity of the membrane

Table 1
Calculated parameters of the test stack with and without PGS at three air flow rates.

	Air flow rate	Maximum power (W)	Corresponding current density (mA cm^{-2})	% Improvement in power	$\sum(E_0)_j$ (V)	$\sum(b)_j$ (mV per decade)	$\sum(R)_j$ (Ω cm^2)	Correlation coefficient
Without PGS	25 slpm	94.0	181	–	9.09	818	10.78	0.993
	35 slpm	103.5	201	–	9.18	791	9.89	0.998
	45 slpm	104.6	201	–	9.20	785	9.58	0.997
With PGS	25 slpm	119.8	221	27.4%	9.09	819	5.27	0.990
	35 slpm	123.5	221	19.3%	9.13	806	4.74	0.997
	45 slpm	123.0	221	17.6%	9.13	812	4.74	0.998

electrolyte. The temperature measurements are consistent with the polarization curves.

Note that the experiments were not conducted in the optimal conditions of the PEMFC stack. Our purpose herein was to introduce the use of PGS to the thermal management of a PEMFC stack and study its feasibility. As known, the membrane water content needs to be sufficient for a PEMFC unit to achieve a satisfactory power output. In the present experiments, hydrogen is fed dry to the anode. PEM hydration is achieved mainly by diffusion flux along the water concentration gradient between the anode and the cathode. The insufficient hydration of the membranes yielded the low efficiency of the stack in the current experiments, with and without PGS, even though the air was humidified to 80% RH at 65 °C. The experimental works of Jang et al. [17] and Yan et al. [18] provide useful information to realize optimal operating conditions on the performances of the PEMFC stack and will be good references for the future study.

The variation of the local current density is strongly dependent on the variation of the local water concentration. Since water is a product of the fuel cell reaction, the water concentration increases along the length of the flow channels from the inlet to the outlet [15,19], when using the present bipolar plates with three-parallel-channel serpentine flow fields for both cathode and anode (Fig. 2). As a result, both the membrane hydration and the water activity increased along the flow path. The local current density increases in the streamwise direction accordingly, so does the local temperature. If the water concentration keeps increasing, water condensation tends to yield the local water flooding of the cathode and worsen local performance, especially in the case with relatively low cell temperature. Increasing the air flow rate removes more water and alleviates the problem of flooding. The observation of trains of visible water drops and plugs in the transparent tube connected at the cathode outlet of the stack in the experiments indicates that water flooding should have occurred in the later section of the serpentine channel at all three flow rates without PGS. The amount of water at the outlet stream shows more serious flooding in the cases at lower flow rates. Note that the cell temperatures at the flow rate of 25 slpm without PGS (Fig. 6) are very close to the inlet gas temperature and the later section of the small serpentine channel is vulnerable to serious water flooding. This observation is consistent with the polarization curve performance and clearly reveals the better polarization curve performance at an air flow rate of 45 slpm than at 25 slpm without PGS, as described earlier.

We interpret the better polarization curve performance with PGS than without PGS as follows. In the experiments herein, PGS is utilized to transport heat effectively out of the PEMFC through conduction, and then to dissipate the heat to surrounding air through the extended fin area by natural convection. The idea is to introduce PGS to positions where the heat generation is high in a PEMFC stack to provide effective cooling and create a more uniform cell temperature inside the stack. As mentioned earlier, since dry hydrogen was supplied in the experiments, all of the water needed in the membrane came from the cathode gas flow, including the water produced by the electrochemical reactions. Both the membrane hydration and the water activity increased along the flow path that brought in the increase of both local current density and temperature in the streamwise direction consequently. With the insertion of PGS, the larger amount of heat generated in the later section of the serpentine channel was conducted more efficiently (than the case without PGS) toward the upstream section by the high in-plane thermal conductivity of PGS. The spatiotemporal dynamic response of the parallel channel PEMFC followed by this quick thermal conduction is a wave of high temperature propagating toward the inlet. The increasing temperature increases the reaction rate of the electrode process and the ionic conductivity of the membrane electrolyte, and a wave of current density propagates toward the inlet thereafter. A high current density results in a high water production and a high membrane water content state or "ignited state" described by Benziger et al. [19]. This, in turn, increases the performance of the cell. The coupled fluid flow, heat and mass transfer proceed within the test cell and the chain sequence continues until a steady state is reached. Overall, the stack has a higher temperature and better performance, with PGS attached (see Figs. 4 and 6).

The higher temperature also relieves the flooding problem. As shown in Fig. 4, the performance of the stack with PGS attached at air flow rate of 25 slpm is very close those at 35 and 45 slpm. The use of PGS is advantageous under relatively low flow rates. The importance and complexity of the coupled fluid flow, heat and mass transfer are again demonstrated.

3.3. Analysis of electrode process

The performance characteristics of the PEMFC stack and the various voltage losses occurring within stack components can be further examined by the polarization curves of the stack obtained at different cathode flow rates (see Fig. 4). The *V–I* characteristics of a single cell in the low and intermediate current density regions [18] can be represented by the following equation:

$$E_i = E_0 - b\log(i) - iR \quad (1)$$

$$E_0 = E_r + b\log(i_0), \quad (2)$$

where E_i and i are the cell voltage and current density under load from experimental observation, respectively, E_0 the open-circuit voltage (OCV), b the Tafel slope, R the ohmic resistance, E_r the reversible potential and i_0 the exchange current density of the cell. It is well known that a fuel cell unit suffers from three major voltage losses: activation polarization, ohmic polarization and mass transfer polarization [1,21]. At low current density the electrochemical process is mainly controlled by the activation of the electrodes, while at high current density the electrochemical process is mainly controlled by ohmic and/or mass transfer polarization. The Tafel slope b and ohmic resistance R represent the voltage losses due to activation polarization of both electrodes and ohmic polarization, respectively. The activation polarization losses are mainly attributed to oxygen reduction reaction in the cell because the activation polarization losses caused by oxygen reduction on Pt catalyst are much higher than that for hydrogen oxidation. The sluggish

electrode kinetics in the initial activation processes can all contribute to activation polarization losses, involving absorption of reactant species, transfer of electrons across the double layer, desorption of product species, the homogeneity of active sites and the nature of both electrode surfaces. Ohmic Polarization losses prevail over the entire range of current density and result from the resistance to the flow of protons in the electrolyte membrane and resistance to flow of electrons through the stack materials, including electrode materials, electrode backing, current collector plates and contact resistance between various interfaces. Ohmic polarization losses, represented by the third term on the right hand side of Eq. (1), vary directly with current. The mass transfer polarization losses occur over the entire range of current density, due to the transport limitation of reactants/products to or from the catalyst layers. These voltage losses become dominant especially at high limiting currents, when it is difficult to provide enough reactant flow to the reaction sites. Note that Eq. (1) does not take the mass transfer polarization into account where the *V–I* curve departs from linearity.

Chu and Jiang [22] have adapted Eq. (1) to describe the *V–I* characteristics and calculate the electrode kinetic parameters for a PEMFC stack, which is assembled by many single cells in series connection. Since the current flowing to each cell is the same, the total voltage of the stack is then expressed as follows:

$$\sum (E_i)_j = \sum (E_0)_j - (\log(i)) \sum (b)_j - i \sum (R)_j \quad (3)$$

Here, the subscript j represents the order of a single cell in the stack and $\sum$ takes the sum of all single cells.

The electrode kinetic parameters obtained by fitting the experimental data with Eq. (3) at different cathode air flow rates, with and without PGS, are summarized in Table 1. The data points where voltage–current relationship departs from linearity have been neglected while performing the non-linear regression analysis to determine the values of $\sum(E_0)_j$, $\sum(b)_j$ and $\sum(R)_j$. Also shown in Table 1 are the correlation coefficients (R^2 value of the fit). It is clear from the R^2 values (0.990–0.998) in the table that the fitted model parameters represent the experimental data very well. The term $\sum(E_0)_j$ is approximately equal to the OCV of the stack. The values of total ohmic resistance, $\sum(R)_j$ at various flow rates, with and without PGS, vary from 4.74 to 10.78 $\Omega\,cm^2$. The corresponding average ohmic resistance of each cell is in the range of 0.474–1.078 $\Omega\,cm^2$, which is higher than the range of values reported by other investigators [20,23]. The insufficient hydration of the membranes under the current experimental conditions yields the low ionic conductivity of the Nafion membrane electrolyte and the higher ohmic resistance. The values of $\sum(b)_j$ vary from 819 to 785 mV per decade. The average values of Tafel slope of each cell fall in the range of 57–110 mV per decade for Pt/C catalyst reported by Chu and Jiang [22], but are higher than the values reported by other investigators [20,22]. The $\sum(b)_j$ value increases because of the increasing irreversibility of hydrogen oxidation, the rate limiting electrode process.

In the present study $\sum(R)_j$ value decreases with increasing temperature. The results on the stacks with PGS show much smaller $\sum(R)_j$ values. As mentioned in Section 3.2, it is because the ionic conductivity of the Nafion membrane electrolyte increases with increasing humidity, accompanied with the increasing temperature and reaction rate of the electrode process. The spatiotemporal dynamic response of the parallel channel PEMFC followed by the quick thermal conduction of PGS homogenizes and increases the temperature of the PEMFC and reduces the ohmic resistance, comparing with the corresponding case without PGS. At low current density, the major factors affecting the values of $\sum(E_0)_j$ and $\sum(b)_j$ are properties of the electrocatalyst, the cell temperature and the humidification conditions [21]. With the same activation process in all experiments (described in Section 2.3), the ranges of values of $\sum(E_0)_j$ and $\sum(b)_j$ with PGS are approximately the same as that without PGS. Generally, $\sum(E_0)_j$ increases with increasing temperature while $\sum(b)_j$ goes in opposite direction. The small initial temperature differences for different flow rates caused by the activation process yields the trends.

4. Conclusions

This work extends our previous work [15] of application of PGS on a single PEMFC to a 10-cell stack. An experimental investigation of the effects of the PGS on the performance and thermal management of a PEMFC stack is reported for the first time. In this passive approach of PEMFC cooling, the waste heat is transferred by thermal conduction via PGS and then discharged to ambiance effectively. PGS is highly thermal conductive, lightweight, flexible and heat-resistant, and is easily assembled in the PEMFC stack. Therefore, the number of auxiliary cooling components and costs can be reduced and the system can be miniaturized. The weight, volume and backwork of the system are also kept to a minimum. Five PGS are bound to the central five cathode gas channel plates and four thermocouples are embedded on the cathode gas channel plates to estimate the temperature variation in the stack under different operating conditions. PGS effectively homogenizes the temperatures inside the cells and increases the reaction rate of the electrode process and the ionic conductivity of the membrane electrolyte. Results of this study demonstrate promising application of PGS to the thermal management of a fuel cell stack. PGS could provide an innovative and economic means of thermally managing a small-to-medium-sized fuel cell stack.

Acknowledgement

The authors would like to thank the National Science Council of the Republic of China, Taiwan, for financially supporting this research under Contract No. NSC-95-2221-E-006-503.

References

[1] W. Vielstich, A. Lamm, H. Gasteiger, Handbook of Fuel Cells, Fundamentals, Technology and Applications, Wiley, 2003.
[2] T.V. Nguyen, R.E. White, J. Electrochem. Soc. 140 (8) (1993) 2178–2186.
[3] T.F. Fuller, J. Newman, J. Electrochem. Soc. 140 (5) (1993) 1218–1225.
[4] R. Mosdale, S. Srinivasan, Electrochim. Acta 40 (4) (1995) 413–421.
[5] R. Andrew, X.G. Li, J. Power Sources 102 (2001) 82–96.
[6] K. Tüber, D. Pócza, C. Hebling, J. Power Sources 124 (2003) 403–414.
[7] A. Hakenjos, H. Muenter, U. Wittstadt, C. Hebling, J. Power Sources 131 (2004) 213–216.
[8] X. Yu, B. Zhou, A. Sobiesiak, J. Power Sources 147 (2005) 184–195.
[9] H. Ju, H. Meng, C.Y. Wang, Int. J. Heat Mass Transfer 48 (2005) 1303–1315.
[10] L. Dumercy, R. Glises, H. Louahlia-Gualous, J.M. Kauffmann, J. Power Sources 156 (2006) 78–84.
[11] M. Wang, H. Guo, C. Ma, J. Power Sources 157 (2006) 181–187.
[12] Y.H. Park, J.A. Caton, J. Power Sources 179 (2008) 584–591.
[13] A. Faghri, Z. Guo, Int. J. Heat Mass Transfer 48 (2005) 3891–3920.
[14] R. Rullière, F. Lefèvre, M. Lallemand, J. Heat Mass Transfer 50 (2007) 1255–1262.
[15] C.Y. Wen, G.W. Huang, J. Power Sources 178 (2008) 132–140.
[16] http://panasonic. com/industrial/components/thermal/thm_hsm.htm, Sep., 2007.
[17] J.H. Jang, H.C. Chiu, W.M. Yan, W.L. Sun, J. Power Sources 180 (2008) 476–483.
[18] W.M. Yan, C.H. Yang, C.Y. Soong, F. Chen, M.C. Mei, J. Power Sources 160 (2006) 284–292.
[19] J. Benziger, J.E. Chia, E. Kimball, I.G. Kevrekidis, J. Electrochem. Soc. 154 (8) (2007) B835–B844.
[20] J. Kim, S. Lee, S. Srinivasan, J. Electrochem. Soc. 142 (1995) 2670–2679.
[21] S. Giddey, F.T. Ciacchi, S.P.S. Badwal, J. Power Sources 125 (2004) 155–165.
[22] D. Chu, R. Jiang, J. Power Sources 83 (1999) 128–133.
[23] F. Laurencelle, R. Chahine, J. Hamelin, K. Agbossou, M. Fournier, T.K. Bose, A. Laperriere, Fuel Cells 1 (2001) 66–72.